Efficiency of Different Types of ED-Tether Thrusters

Juan R. Sanmartin[1], Robert D. Estes[2], and Enrico C. Lorenzini[3]

[1]*Escuela Técnica Superior de Ingenieros Aeronáuticos, Universidad Politécnica de Madrid, 28040 Madrid, Spain*
[2,3]*Harvard-Smithsonian Center for Astrophysics, Cambridge, Massachusetts 02138*
[1]*34-91-3366302, jrs@faia.upm.es*

Abstract. The efficiencies of electrodynamic-tether (EDT) thrusters made of single bare tethers with different types of cross sections, several parallel bare tethers, or a fully insulated tether with a three-dimensional passive end-collector, are discussed. Current collection, mass, and ohmic resistance considerations are balanced against each other in discussing efficiencies. Use is made of recent results on the validity domain of orbital-motion-limited (OML) collection, the current law beyond that domain, and interference effects between parallel bare tethers; and on current adjustment to variations in electron density encountered in orbit. Comparisons between EDT thrusters and electrical thrusters in terms of the ratio of dedicated mass to the total mission impulse show EDT to be superior for mission times over 50-100 days.

INTRODUCTION

The basic figure of merit for a thruster is the ratio $M_d/F\tau$, which is the inverse of a velocity, and should be as small as possible. Here, F is thrust, τ is duration of thrusting, and M_d is dedicated mass. For electrical thrusters, which would be natural competitors of tethers, M_d is made of propellant mass $\dot{m}_p\tau$ ($\dot{m}_p \equiv$ propellant flow rate) and tankage and plumbing mass ($\alpha\dot{m}_p\tau$); and from hardware related to the required electrical power W_e,

$$M_d = \dot{m}_p\tau(1+\alpha) + \beta W_e \ . \tag{1}$$

Typically, α is about 0.2, and β is about 6 kg/kW if just power processing unit and thruster need be considered and one order of magnitude greater if dedicated solar panels are required (Martinez-Sanchez and Pollard, 1998; Estes et al, 2000).

Introducing the specific velocity v_{sp} (specific impulse in velocity units, about 16 and 28 km/s for Hall and Ion thrusters respectively), one has $\dot{m}_p = F/v_{sp}$ and $W_e = Fv_{sp}/2\eta$ (η = thruster efficiency = 0.5-0.65), and arrives at

$$\frac{M_d}{F\tau} = \frac{1+\alpha}{v_{sp}} + \frac{\beta v_{sp}/2}{\tau\eta} \ . \tag{2}$$

Given a specific velocity, the ratio $M_d/F\tau$ approaches a limit minimum for long thrust durations, with a characteristic time $\tau \propto v_{sp}^2$. Duration, however, may need be restricted by a number of reasons. For each maximum allowed τ, there is an optimal specific velocity yielding a minimum in (2); as τ is allowed to increase, v_{sp}(opt) increases, resulting in a lower $M_d/F\tau$ minimum. In addition, given a total (mission) impulse $F\tau$, a maximum allowed duration determines a lower bound for thrust F.

CP552, *Space Technology and Applications International Forum–2001*, edited by M. S. El-Genk

THE BARE-TETHER THRUSTER

At the top of a thrusting tether there is a power supply to push current down against the induced electric field E_m (Fig.1). There is also an electron-ejecting hollow cathode; its bias ΔV_{hc} typically amounts to a few percent of the full induced bias E_mL (L = tether length), and will be neglected here. One then has

$$M_d = \dot{m}_{hc}\tau(1+\alpha) + \beta W_e + \alpha_t M_t, \tag{3}$$

where $\dot{m}_{hc}$ is now the expellant flow rate at the hollow cathode; α and β are as in Sec.1; and $M_t = LA_c\rho^*$ is the tether mass ($\rho^* = \rho_c + \rho_n A_n/A_c$, with A_c and A_n conductive and nonconductive cross-section areas of densities ρ_c and ρ_n respectively). A factor α_t = 2-3 accounts for the mass of related hardware (end ballast-deployer). For an optimal design the deployer serves as the end ballast, and an α_t = 2 might be achieved. We have assumed such an optimization in much of the following.

With U_{sat} the satellite velocity, I_C the electron current at the tether top, and $W_m = FU_{sat}$ the thrusting power, we have

$$\frac{M_d}{F\tau} = \frac{1+\alpha}{\omega_{hc} \times W_m / E_m I_C} + \frac{\beta U_{sat}}{\tau}\left[\frac{1}{\eta} + \frac{\alpha_t \rho^* / \beta\sigma E_m^{\,2}}{w}\right], \tag{4}$$

where σ is conductivity, ω_{hc} is a frequency determined by the normal component of the geomagnetic field and by a 'charge-to-mass' ratio equal to the hollow-cathode ratio of current to mass-flow-rate,

$$\omega_{hc} = (I_C / \dot{m}_{hc}) \times E_m / U_{sat}, \tag{5}$$

and η and w (a measure of thrusting power per unit tether mass) are given by

$$\eta \equiv W_m / W_e, \qquad w \equiv (\rho^* / \sigma E_m^{\,2}) W_m / M_t. \tag{6a, b}$$

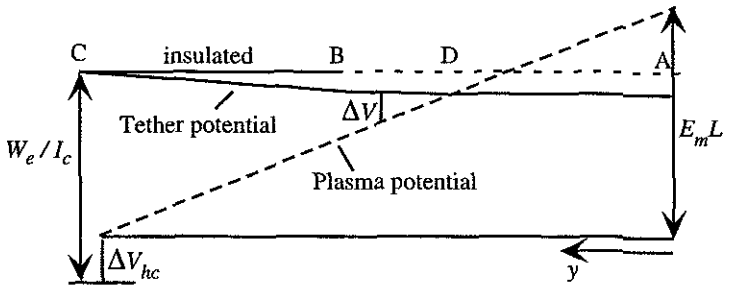

FIGURE 1. Tether Voltage Diagram.

Figure 1 shows the configuration of a thruster system using a bare tether. The bias ΔV varies along the tether due to both induced and ohmic voltage drops,

$$d\Delta V / dy = E_m + I / \sigma A_c. \tag{7}$$

An upper segment BC of length L_i is insulated to increase the operating efficiency. In general, the bias at end point A will vary along the orbit; we will first assume $\Delta V_A < 0$. Electrons are thus collected over a segment DB, with D the varying zero-bias point. Since the current vanishes at A, and (ion) collection along the segment AD is negligible, we may set $I_D = 0$. An analysis of bias and current profiles along the tether is needed to fully determine W_m/E_mI_C, η, and w in Eq.(4):

i) Taking the current $I(y)$ from (7) one first finds

$$W_m = E_m \int_D^C I(y)dy = \sigma E_m A_c \left[\frac{W_e}{I_C} - E_m (L_i + L_{DB}) \right]. \tag{8}$$

ii) Next, we integrate Eq.(7) from B to C with $I = const = I_B = I_C$ to find

$$W_e / I_C = \Delta V_B + L_i (E_m + I_C / \sigma A_c). \tag{9}$$

iii) Between D and B the current is given by the OML law, modified by a factor G if needed,

$$dI / dy = (p / \pi) G e N_\infty \sqrt{2e\Delta V / m_e}, \tag{10}$$

with N_∞ the ionospheric plasma density and p the perimeter of the tether cross section. Space-charge effects on the current, for cross sections too thick, are described by a factor G that is nearly independent of bias for the values of interest (Estes and Sanmartìn, 2000); we shall assume that this also applies to a factor G describing other non-OML effects, if any, making G independent of y in (10), for a simpler analysis. We may then introduce convenient dimensionless variables,

$$i \equiv I / \sigma E_m A_c, \qquad \xi \equiv y / L^*, \qquad \varphi \equiv \Delta V / E_m L^*,$$

with a characteristic length L^* defined by

$$L^* G \frac{p}{\pi} e N_\infty \sqrt{\frac{2eE_m L^*}{m_e}} = \frac{3}{4} \sigma E_m A_c. \tag{11}$$

Note that L^* varies (basically with N_∞) along the orbit. Equations (7), (10) now become

$$d\varphi / d\xi = 1 + i, \qquad di / d\xi = 3\sqrt{\varphi} / 4,$$

with a first integral, $\varphi^{3/2} - (2i + i^2) = \text{const} = 0$, and the constant evaluated at point D (Sanmartín, Martínez-Sánchez and Ahedo, 1993). At point B this first integral yields

$$\varphi_B = (2i_C + i_C^{\,2})^{2/3}; \tag{12}$$

also the first integral can be used to integrate the bias equation from D to B, giving

$$\frac{L_{DB}}{L^*} = \int_0^{\varphi_B(i_C)} \frac{d\varphi}{\sqrt{1 + \varphi^{3/2}}}. \tag{13}$$

We can now use Eqs.(8), (9) and (13) to first write

$$W_m / E_m I_C = L_i + q(i_C) \times L^*, \tag{14}$$

with $q(i_C)$ given by

$$q \equiv \frac{1}{i_C} \left[\varphi_B(i_C) - \int_0^{\varphi_B(i_C)} \frac{d\varphi}{\sqrt{1 + \varphi^{3/2}}} \right] \tag{15}$$

and $\varphi_B(i_C)$ given by Eq.(12). Next, using (9) and (14), we can write

$$\frac{1}{\eta} = \frac{1 + i_C + \lambda \varphi_B(i_C)}{1 + \lambda q(i_C)}, \tag{16a}$$

$$\frac{1}{w} = \frac{L / L_t}{i_C[1 + \lambda q(i_C)]}, \tag{16b}$$

where we have $L \geq L_i + L_{DB}$, or

$$\frac{L}{L_i} \geq 1 + \lambda \times \int_0^{\varphi_B(i_C)} \frac{d\varphi}{\sqrt{1 + \varphi^{3/2}}}, \tag{17}$$

and where we have defined

$$\lambda \equiv \frac{L^*}{L_i} = \left[\frac{3\pi}{4\sqrt{2}} \frac{m_e^{1/2}}{e^{3/2}} \frac{\sigma \sqrt{E_m} A_c}{N_\infty L_i^{3/2} p} \right]^{2/3}. \tag{18}$$

In Eqs.(14),(16a,b), i_C is determined in terms of λ and (dimensionless) supplied power $W_e / \sigma E_m^2 A_c L_i$,

$$i_C\left[1 + i_C + \lambda\left(2i_C + i_C^2\right)^{2/3}\right] = \frac{W_e}{\sigma E_m^2 A_c L_i}. \tag{19}$$

COMPARISON OF EDT AND ELECTRICAL THRUSTERS

Before considering the details of optimal tether design, let us compare the extended-mission mass requirements of some typical electrical thrusters with that of bare-tether thrusters chosen to have equivalent average thrust. There are two cases to consider: the case where a dedicated solar power system is required, which would be the case for any kind of electrical orbit-transfer vehicle (a space "tug"); and the case where the solar power system is already in place, with power available for thruster use, which might be the case for a Space Station drag-compensation system.

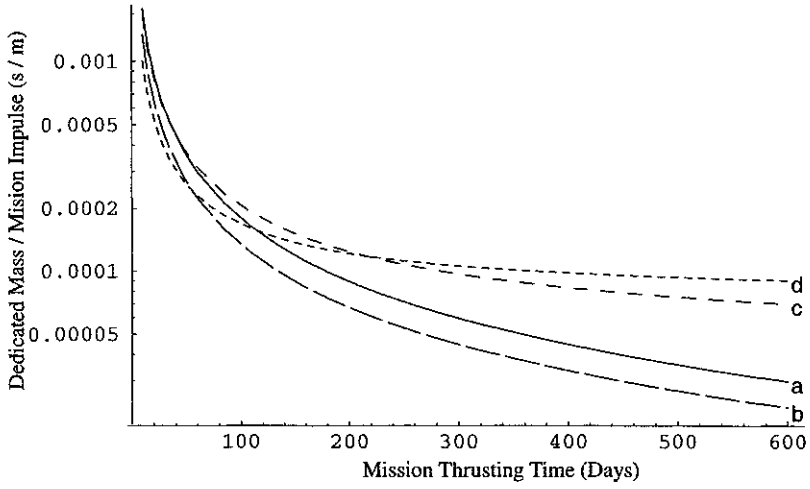

FIGURE 2. Comparison of EDT (a, b) and Electrical Thrusters (c, d) With Dedicated Solar Power System.

Fig. 2 shows the case where a dedicated power system is required. It plots $M_d / F\tau$ on a logarithmic scale for a range of mission (thrusting) times τ of 10 to 600 days. All systems are taken to have $\eta = 0.6$. Curves c and d correspond to electrical thrusters of $v_{sp} = 28$ and 16 km/s, respectively. The EDT systems were chosen to provide an average η of

0.6 over an altitude range of 300 to 800 km. Curve a is for a 30 kg tether (with $\alpha_t = 2$) and $W_e = 1$ kW. Curve b corresponds to the same tether but with $W_e = 2$ kW; it is seen to be better than either electrical thruster for mission times of roughly 50 days or more, while the upper EDT (1 kW) curve needs a mission time of over 120 days to achieve that. Both of these times are well within the time required for either type of system to boost a large payload from one low Earth orbit to another orbit several hundred kilometers higher.

Multiple orbit transfers would, of course, take proportionally longer, and the time to return to lower orbit would also have to be taken into account. We note that by only considering powered thrusting, we have, so to speak, forced the EDT to fight with one hand tied behind its back, since the EDT does not require external power to descend to a lower orbit. An orbit-transfer vehicle would need to return to a lower orbit after taking a spacecraft to a higher one, and an EDT system could, if so designed, descend more quickly than its electrical thruster counterpart. This is a topic for later development. There are implicit assumptions of system lifetimes and practicality of the systems which we note without further discussion.

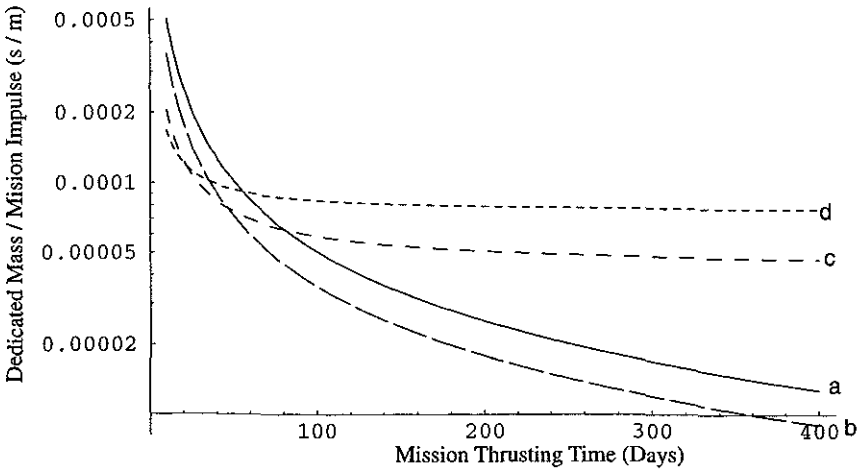

FIGURE 3. Comparison of EDT (a, b) and Electrical Thrusters (c, d) Without Dedicated Solar Power System.

As Fig. 3 shows, for the case where abundant power is available without the need for a dedicated solar system, the EDT is clearly superior to the electrical thrusters for mission lifetimes somewhat shorter than for the case when a dedicated system is required. All parameters for the electrical thrusters c and d are the same as for Fig. 2, except for β. The tethers have a mass of 70 kg, and the assumed operating power is 5 kW for curve a and 10 kW for curve b. Thus, as previously noted (Estes et al., 2000), EDT would be attractive for International Space Station (ISS) reboost, assuming power were available from the Station.

TETHER DESIGN

Now we turn to optimal EDT design. Ignoring considerations other than those discussed above, Eq.(4) shows that making the tether nonconductive over part of the cross section puts a mass penalty on the system ($M_d/F\tau$ increases); we shall thus take $\rho^* = \rho_C$ in the following. Also, we shall assume that the tether is designed for the equal sign in (17) to apply at some nominal environmental conditions (point D at end A in Fig.1). Finally, we shall take $G \approx 1$, assuming OML current throughout (see discussion below).

Note now that both ω_{hc} *times length* W_m/E_mI_C ($\equiv v_{sp1}$) and $2U_{sat}$ ($\equiv v_{sp2}$) play the role of specific velocitiy in Eq.(4), when compared with (2). For Xenon expellant we have

$$v_{sp1} \approx 350 \frac{km}{s} \times \frac{I_C(Amp)}{\dot{m}_{hc}(sccm)} L_t(km) \times [1 + \lambda q(i_C)],$$

where the flow rate is measured in standard cubic centimeters per minute. For typical values $I_C(Amp)/\dot{m}_{hc}(sccm) \sim 1$, and length L_t of several kilometers, v_{sp1} is about two orders of magnitude greater than the specific velocities of electrical thrusters, whereas v_{sp2} is comparable. This means that for τ such that an electrical thruster reaches around its $M_d/F\tau$ minimum, a tether will attain a much lower $M_d/F\tau$ ratio (unless either η or w in (4) is very small) For that ratio to reach its tether minimum, however, unreasonably long times might be required; in a sense, v_{sp1} might then be taken as infinite in Eq.(4). Tether design should then strive to reduce the quantity within the bracket in (4), which is an overall inverse efficiency for the tether,

$$\frac{1}{\eta(\lambda, i_C)} + \frac{\gamma}{w(\lambda, i_C)} \equiv \frac{1}{\eta_t}. \tag{20}$$

In Eq.(20) we have considered nominal conditions (equal sign in (17)) and defined

$$\gamma \equiv \alpha_t \rho_c / \beta \sigma E_m^{\,2}. \tag{21}$$

Taking ρ_c(Al) = 2.7×10^3 kg/m^3 and σ(Al) = $3.5\times10^7/\Omega$×m, α_t =2.25, and a representative nominal value E_m = 120 V/km, Eq.(21) gives $\gamma = 2$ (0.2) for $\beta = 6$ kg/kW (60 kg/kW).

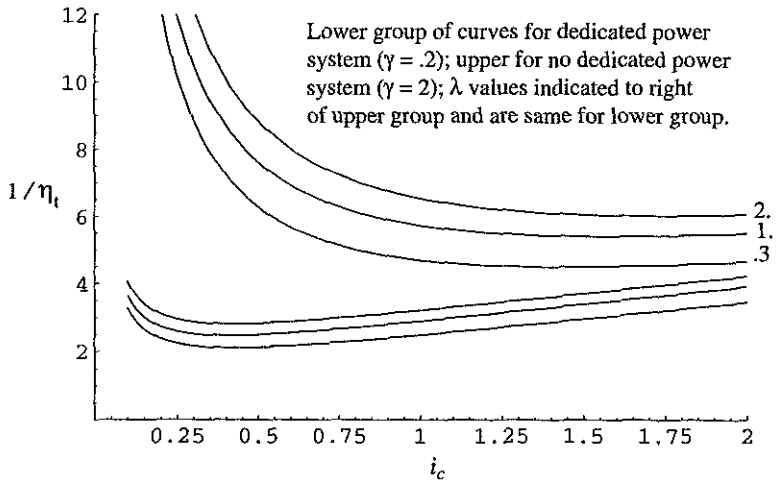

FIGURE 4. Overall Inverse Tether Efficiency Versus i_C

Fig. 4 shows the overall inverse efficiency $1/\eta_t(\lambda,\gamma,i_C)$. For given λ and γ, all curves present a minimum (maximum of η_t) at some particular, optimal i_C; that minimum decreases with both λ and γ. For small λ (corresponding to negligible collection impedance), limit laws $1/\eta = 1 + i_C$, $w = i_C$, reflect the fact that mass ($\propto A_c$), and ohmic impedance ($\propto 1/A_c$) and thus inverse power efficiency η, vary with section area in opposite ways, and give rise to the extremum. At $\lambda \approx 0$, we have

$$\eta_t = \eta_t^{\,max} \approx \frac{1}{1+2\sqrt{\gamma}} \qquad at \quad i_C \approx \sqrt{\gamma}, \tag{22}$$

$$\rightarrow \quad \eta_t^{\,max} \approx 0.53\ (0.26) \qquad at \quad i_C = 0.45\ (1.41) \qquad for \quad \gamma = 0.2\ (2).$$

At $\lambda = 1$, Fig.4 gives $\eta_t^{\,max} \approx 0.40$ (0.18) for $\gamma = 0.2$ (2).

In addition to higher efficiency, a low λ value makes tether performance less sensitive to N_∞ variations in orbit. To make λ low in Eq.(18) one may use a thin tape (ratio $A_c/p \approx h/2$, $h \equiv$ thickness) with a long insulated segment. There will be limitations, however, on how thin and long a tether might be. Taking, for example, h = 0.2 mm, and a nominal value $N_\infty = 3\times10^{11}$ m^{-3} one finds $L^* \approx 2.16$ km; taking then $L_t = 4$ km, say, we have $\lambda \approx 0.54$, yielding $\eta_t^{\,max} \approx$ 0.47 (0.22) for $\gamma = 0.2$ (2). Thus the second terms in (2) and (4) are of the same order of magnitude.

Note that given λ and γ there is still considerable freedom in choosing a design value for i_C because the minima in Fig.4 are very flat, allowing us to take i_C well away from the minimum with little effect on η_t. This may be useful in tether design because, as seen below, taking i_C as low as possible (corresponding to low ohmic impedance) makes performance less sensitive to E_m variations. Also, moving to the left of the minimum trades electrical power against tether mass at fixed thrust, and again serves design, which, in addition to needing to keep η_t high, will face restrictions on the power available W_e.

For the conditions leading to $\lambda \approx 0.54$ and $\gamma = 0.2$ above, one may reasonably set i_C as low as 0.25 in Fig.4 yielding $L/L_i \approx 1.34$ in Eq.(17) (with the equal sign), and $L \approx 5.3$ km. The thrust F now depends on just the cross section A_c, as follows from using Eqs.(16a) and (19) to write

$$\frac{U_{sat}F}{\sigma E_m^{\,2} L} = A_c \times i_C \frac{L/L_i}{1+\lambda\, q(i_C)}. \tag{23}$$

For example, a 10 mm tape width, leading to $A_c \approx 2$ mm^2, yields $F \approx 0.15$N, $M_t = 28.6$kg, and $W_e = 1.63$ kW. For the conditions leading to $\lambda \approx 0.54$ and $\gamma = 2$ above, one may reasonably set $i_C = 0.75$, yielding $L/L_i \approx 1.68$ and $L \approx 6.7$km; a 6mm width ($A_c \approx 1.2$ mm^2) now yields $F \approx 0.31$ N, $M_t = 21.7$ kg and $W_e = 4.77$ kW.

To consider off-nominal conditions we now write Eq.(20) as

$$1/\eta_t = (1 + \alpha_t M_t/\beta W_e)\times 1/\eta.$$

In the simplest scheme we keep supplied power W_e constant as environmental conditions change along the orbit. Changes in η then reflect on proportional changes in both $\eta_t = \eta \times const$ and thrust, $F = \eta \times W_e/U_{sat}$. We use Eq.(19) to find how i_C changes with either N_∞ or E_m, and then use (16a) to find changes in η.

Consider first plasma density effects. For the nominal conditions discussed above, a density rise to 10^{12} m^{-3} (about maximum) leads to $L^* \approx 0.96$km, and $\lambda \approx 0.24$. For the $\gamma = 0.2$ case, i_C changes in Eq.(19) from the previous value 0.25 to 0.28; then η (and thus η_t and F) increases in (16a) by just 6%. For the $\gamma = 2$ case, i_C changes in (19) from 0.75 to 0.86; then η, and η_t and F, increase by just 3%. Note that point D will now lie above tether end A in Fig.1. Looking at the reverse length increase of segment BD, as N_∞ drops back from 10^{12}m^{-3} to 3×10^{11} m^{-3}, the small reverse decreases in both η_t and F show the ability of bare tethers to accommodate electron density variations (Estes, Sanmartín, and Martínez-Sánchez, 2000). If N_∞ drops to a value 10^{11} m^{-3}, leading to $L^* = 4.5$km and $\lambda \approx 1.12$, the tether accommodates too, ΔV_A becoming positive. Expressions, for this case, of either η or w, which were given by Sanmartín, Martínez-Sánchez, and Ahedo (1993), will not be discussed here.

Induced field variations are smaller, but their effects are stronger, though still moderate. For the nominal conditions discussed above, an E_m decrease from 120 V/km to 80 V/km, say, leads to $L^* \approx 1.88$ km, and $\lambda \approx 0.47$. The greater effect in Eq.(19) arises from the $E_m^{\,2}$ factor. For the $\gamma = 0.2$ case, i_C changes in (19) from the previous value 0.25 to 0.46; then η (and thus η_t and F) decreases in (16a) by just 14%. For the $\gamma = 2$ case, i_C changes in (19) from 0.75 to 1.27; then η, and η_t and F, decrease by about 21%.

To conclude, note that using a tether of circular section with ratio A_c/p (=*radius*/2) = 0.1 mm, as the tape above (same λ), would result in very small A_c (0.126 mm^2) and very small thrust in Eq.(23). A cylindrical aluminum shell of outer radius 1.66 mm and inner radius 1.55 mm would be the exact equivalent of the tape. In practice, however, the interior of such a tether would need to be filled with some low-density material, which would increase its mass by a significant amount. Thus, the tape geometry is the clear winner from the standpoint of thrust per mass. Tapes could be as wide as 12 mm and reach $A_c = 2.4$ mm^2 for a 0.2 mm thickness. That width is about four times the minimum Debye length found in orbit, ensuring OML collection ($G \approx 1$) throughout (Sanmartín and Estes, 1999). The current stays close to OML values at somewhat larger values of tape width in a quiescent plasma, but ion ram-energy effects suggest conservative design should not exceed the 4-times-Debye length bound on width (Estes and Sanmartín, 2000).

Since tether length L will be restricted by a variety of reasons, increasing tether thrust in (23) by one order of magnitude, say, would require moving into section areas one order of magnitude greater by increasing tape width. In practice one would finally reach circular cross sections. Maximum area might then be achieved using a circle with radius equal to the minimum Debye length (~3 mm at $N_\infty \sim 10^{12}\,\mathrm{m}^{-3}$), giving $A_c \approx 30\ \mathrm{mm}^2$. The accompanying A_c/p increase would greatly reduce efficiency, however. This suggests using multiple tethers, each with a low A_c/p ratio to keep efficiency high, when high thrust is required. Interference effects between parallel tethers has recently been proved moderate (Sanmartín and Estes, 2000).

Fully Insulated Tether with Anodic End-Collector

Results for a fully insulated tether, equivalent to Eqs.(14), (16a, b), (19), (20), and (23), are quite simple because current is now constant along the tether ($I = const = I_C$); one readily finds

$$W_m / E_m I_C = L, \qquad 1/\eta = 1 + i_C + \Lambda^2 {i_C}^2, \qquad 1/w = \gamma_b / i_C, \tag{24a-c}$$

$$\frac{1}{\eta_t} = 1 + i_C + \Lambda^2 {i_C}^2 + \frac{\gamma\gamma_b}{i_C}, \qquad \frac{U_{sat} F}{\sigma {E_m}^2 L} = A_c \times i_C, \tag{25a, b}$$

with $i_C(\Lambda,\ W_e/\sigma {E_m}^2 A_c L)$ determined by

$$i_C(1 + i_C + \Lambda^2 {i_C}^2) = W_e / \sigma {E_m}^2 A_c L. \tag{26}$$

Note that the fully insulated tether does require an electron collector at its anodic end, say a passive spherical collector, lying at the bottom (right) in Fig.1. We thus wrote

$$\alpha_t \rightarrow \alpha_t \gamma_b \equiv \alpha_t (1 + \alpha_b M_b / \alpha_t M_t)$$

in Eqs.(3) and (4), the factor γ_b accounting for the mass of the collecting balloon, and its own deployer through another coefficient, $\alpha_b > 1$; this results in Eq.(24c). The Λ terms in (24b), (25a), and (26) originate in the current characteristic for the balloon, $I_C(\Delta V_A)$, for which we used a semi-empirical law extracted from the TSS1-R tether results (Vannaroni et al, 1998),

$$I_C = A_b \times e N_\infty \sqrt{kT_e / 2\pi m_e} \times \left[(\lambda_{De} / R)^{4/3} e\Delta V_A / kT_e \right]^{a_1} a_2, \tag{27}$$

with $A_b = 4\pi R^2$ and R the balloon radius, T_e the electron temperature, λ_{De} the Debye length, and $a_1 = 0.472$, $a_2 = 4.826$. For our discussion we may set $a_1 = 1/2$, yielding $\Delta V_A \propto {I_C}^2$. We then find

$$\Lambda \equiv \frac{\sqrt{2\pi}}{a_2} \times \left(\frac{R}{\lambda_{De}} \right)^{2/3} \times \frac{{m_e}^{1/2}}{e^{3/2}} \frac{\sigma \sqrt{E_m} A_c}{N_\infty \sqrt{L} A_b}. \tag{28}$$

To properly compare a fully insulated tether to a partially bare tape, we set common values of tether length L, thrust F (as it results from common values for both total mission impulse and thrust duration), and nominal conditions for N_∞, E_m, and σ. This makes the left hand sides of (23) and (25b) equal. We will consider a balloon radius of 2m and a temperature of 0.1 eV, making Λ just proportional to the free value of A_c in (28). Note now that the $\Lambda^2 {i_C}^2$-term in (25a) is independent of our choice for A_c, the product $A_c i_C$ being fixed in Eq.(25b) by its left-hand-side. For nominal conditions and L, F values as in the examples of the previous section, we find $A_c i_C$ in (25b) must equal 0.45 mm^2 (0.74 mm^2) for $\gamma = 0.2$ (2), giving

$$\Lambda i_C \approx 2.32\ (3.39) \quad for \quad \gamma = 0.2\ (2).$$

Taking $\gamma_b = 2$ in (25a) we find $\eta_t^{max} \approx 0.13$ (0.061) for $\gamma = 0.2$ (2); this represents moree than a half order of magnitude drop in efficiency with respect to the tapes.

We add some further comments: *i*) The empirical current law (27), based on TSS-1R data, would overestimate the current when applied to spheres larger, and densities lower, than those corresponding to the TSS1-R flight, for magnetic effects would then be dominant. *ii*) The fully insulated tether would not accommodate drops in density, say from 3×10^{11} to 10^{11} m^{-3}. *iii*) As tape section area A_c is increased beyond 1-2 mm^2, the fully insulated tether looks progressively worse. *iv*) There is no sensible way of using multiple balloons of 2 m radius, to accommodate future large-thrust requirements.

CONCLUSIONS

In terms of total mass required for the mission, EDT thrusters are superior to electrical thrusters for mission thrusting times of 50-100 days or more both in the case of dedicated solar panels and the case when power is available without the need for a dedicated system. The advantage becomes greater as the mission time increases because of the comparatively insignificant use of gas by the EDT systems. Since an EDT tug would require no electrical power to descend, one could be designed to improve the mass to mission impulse ratio by descending at a rate faster than it ascends in the electrically powered mode, thus increasing its advantage over electrical thrusters.

We have obtained equations to guide bare-tether system design. Our analysis shows that one can generally design a system that is close to the optimum, whatever the constraints of available power or orbit of operation. Tape or ribbon tethers were seen to be the most efficient design for obtaining maximum thrust within a given mass budget. Parallel tethers appear to be useful only when required thrust levels cannot be achieved by a single tether within tether length restrictions. End-collector (insulated wire) anodes were seen to be substantially worse than bare tethers in terms of mass versus thrust. Many other factors have to be considered in final decisions of electrical thrusters versus EDT, including required maneuverability, system lifetime, and mission lifetime.

ACKNOWLEDGMENTS

The work of Estes and Lorenzini was supported by NASA Grant NAG8-1605 from the Marshall Space Flight Center. The work of Sanmartín was supported by the Comision Interministerial de Ciencia y Tecnología of Spain, Grant PB97-0574-C04-1.

REFERENCES

Estes, R. D., and Sanmartín, J. R., "Cylindrical Langmuir Probes Beyond the Orbital-Motion-Limited Regime," *Phys.Plasmas* **7**, pp. 4320-4325 (2000).

Estes, R. D., Sanmartín, J. R., and Martínez-Sánchez, M., "Performance of Bare-Tether Systems Under Varying Magnetic and Plasma Conditions," *J.Spacecraft & Rockets* **37**, pp. 197-204 (2000).

Estes, R. D et al., "Bare Tethers for Electrodynamic Spacecraft Propulsion," *J.Spacecraft & Rockets* **37**, pp. 205-211 (2000).

Martínez-Sánchez, M., and Pollard, J. E., "Spacecraft Electric Propulsion—An Overview," *J.Prop.Power* **14**, pp. 688-699 (1998).

Sanmartín, J. R., Martínez-Sánchez, M., and Ahedo, E., "Bare Wire Anodes for Electrodynamic Tethers," *J.Prop.Power* **9**, pp. 353-360 (1993).

Sanmartín, J. R., and Estes, R. D., "The Orbital-Motion-Limited Regime of Cylindrical Langmuir Probes," *Phys.Plasmas* **6**, pp. 395-405 (1999).

Sanmartín, J. R., and Estes, R. D., "Collection Effects on Close Parallel Bare Tethers," **AIAA 2000-1073**, *38th Aerospace Sciences Meeting & Exhibit* (2000).

Vannaroni, G. et al., "Current-voltage Characteristic of the TSS-1R Satellite: Comparison with Isotropic and Anisotropic Models," *Geophys.Res.Lett.* **25**, pp. 749-752 (1998).